Progress In Electromagnetics Research C, Vol. 106, 29–44, 2020

Small-Cell Waveguide Antenna Array for E-Band Point to Point Wireless Communications

Mamadou B. Gueye and Habiba Hafdallah Ouslimani*

Abstract—In this paper, a highly directive small-cell waveguide antenna array for point to point wireless communication in E-band radio frequency systems is presented. The antenna array is designed and dedicated for the paired bandwidths 71–76 and 81–86 GHz. It is composed of 32×32 horn elements with a total surface of $\sim 100 \times 100\,\text{mm}^2$ to achieve a directivity $\geq 38\,\text{dB}$, narrow beam ($\sim 2^\circ$), and low-level sidelobe $\leq -26\,\text{dB}$. A compact stepped horn antenna element (SHE) (6.6 mm) is designed. It is 25% smaller than a standard horn element (in the same band) keeping the same aperture surface ($3.4 \times 3.4\,\text{mm}^2$). Layer-by-layer micromachining process is employed for the fabrication. A compact feeding network (25 mm) is realized using ridged waveguide technique with a cut-off frequency of 55 GHz, much lower than standard WG one in the same band. A bow-tie multi-section waveguide polarizer rotator ($\pm 90^\circ$) is optimized and associated with the WG transitions to re-phase the fields applied to SHE elements. Electric discharge machining (EDM) process was used to manufacture a 4×4 sub-array prototype including the entire WG power-feed network. The antenna is characterized in an anechoic chamber, and experimental results are compared to 3-D electromagnetic simulations with good agreements over the two bands.

1. INTRODUCTION

In recent years, the paired frequency bands of 71–76 GHz and 81–86 GHz, commonly known as E-band, have attracted a lot of interest for ultra-high capacity wireless communications [1–17]. Such large available bandwidth (5 GHz for each band) provides multi-gigabit rate point-to-point wireless transmission capabilities. This paves the way to various applications in millimetre Wave (mm-Wave) domain including local area network (LAN), high speed broadband metropolitan links, 5G communications, wireless backhaul systems of mobile cellular networks, intelligent transport system, anti-collision radar, etc. [4–26]. We notice that the radar is a bit different from high bit rate communication systems. It uses the same frequency in transmission and reception, but high bit rate communication systems use two sub-bands. These mm-Wave applications require highly directive antennas with compact dimensions for better integrations in the electronic modules. Moreover, in order to be deployed in the future urban and suburban areas, the antenna array must satisfy the European Telecommunications Standards Institute (ETSI) [27] requirements over 71–86 GHz band. Antennas of large dimensions are usually deployed to obtain very high gain and small beamwidth angle such as the commercial E-Band parabolic antennas (HPCPE-80) [28] having dimensions of $640 \times 410 \times 330\,\text{mm}^3$, the Cassegrain antenna using a Fresnel flat reflector having a diameter of ~ 300 mm, as well as the cylindrical reflector antennas which have diameters of 190 mm and ~ 62 mm depth [10, 11, 29, 30]. Despite their good performance, the sizes can represent a handicap. Planar antennas using dielectric substrates, in microstrip, multilayered PCB, or substrate integrated waveguide (SIW) technologies can also represent

Received 20 July 2020, Accepted 11 September 2020, Scheduled 6 October 2020

* Corresponding author: Habiba Hafdallah Ouslimani (habiba.ouslimani@parisnanterre.fr).

The authors are with the Electromagnetic Group, Energetic Mechanics Electromagnetism Lab, University Paris Nanterre, Ville d'Avray, 50 rue de SEVRES 92410, France.

low cost solutions for a massive deployment. However, losses may occur at the highest frequencies and in millimeter waves range reducing the gain.

The present work aims to develop a low cost compact size waveguide antenna array over the paired 71–76 and 81–86 GHz bands with broadband features and high directivity. A small-cells planar antenna array composed of 32×32 compact horn elements associated with the entire feeding network is proposed. The key design technique to achieve a full coverage of E band is based on three points. First, the "Stepped horn element" (SHE) [18–20, 31] optimized to be compact, wideband matching impedance and high gain over the entire E-band. The large beamwidth of the SHE (quasi-omnidirectional radiation pattern) is perfect for wide beam scanning. Second, the design ultra-compact feeding network benefits from ridged waveguide techniques which allow smaller wave guide section than the standard WR12. Third, waveguide feeding network has very few losses conjugate to low mutual couplings which is an advantage in mm-Wave in comparison to the microstrip technology which suffers from transmission lines losses and coupling effects, drastically high when the number of elements increases. Several elements such as the stepped horn elements, polarizers, power dividers, and waveguide portions are optimized and successfully implemented. The polarization rotation components ($\pm 90°$ rotation or twisters) have a total height of ~ 1.6 mm. Based on two bow-tie sections [32–36], they are successfully implemented in the waveguide supply network with a measured return loss higher than 30 dB and insertion loss lower than 0.2 dB from 71 to 86 GHz. The 3 dB power dividers and WG transitions are designed using ridged waveguide technique with smaller rectangular section sizes ($a \times b$: $2.3 \times 1.0\,\text{mm}^2$) than that of the standard WR12 ($a' \times b'$: $3.0988 \times 1.5494\,\text{mm}^2$). The measured cut-off frequency is $F_C = 55$ GHz, much lower than the cut-off frequency ($= 65$ GHz) of standard waveguide devices with the same section. They present low insertion losses and total energy transfer in E-band.

The 32×32 proposed antenna achieves a minimum directivity of > 38 dB, a large matching impedance bandwidth (i.e., $|S_{11}| < -10$ dB) from 71 GHz to 86 GHz, low cross-polarization and SLL, and high Front to Back Ratio (F/B ~ 45 dB) with global sizes of $L \times W \times H = 108 \times 108 \times 25\,\text{mm}^3$.

An experimental demonstrator based on a subarray of 4×4-elements was designed, fabricated, and characterized. The antenna achieves high directivity and promising frequency behaviours in the E-band suggesting a potential use as point-to-point wireless communication platform. 3D printing technology [37, 38] should facilitate the realization of this ultra-compact antenna (32×32 elements) in a single monolithic block. This leads to the objective of integrability in mm-Wave modules at low cost. The paper is organized as follows: Section 2 presents the design, realization, and experimental results of the Stepped Horn Element (SHE). Section 3 details the design of the antenna array. Section 4 presents the experimental characterization of the 4×4 array and comparison with the simulation results. Finally, Section 5 gives the conclusion.

2. STEPPED HORN ELEMENT (SHE) DESIGN AND CHARACTERIZATION

Figure 1 shows the proposed new compact stepped horn antenna (SHE). It is composed of five rectangular waveguide sections with different dimensions flared in steps and stacked along the direction of propagation. The technique of stepped or discretized horn antenna was used in [20] to the analysis of corrugated horns with an arbitrary geometry and without any restriction on the profile or the flare angles of the horn. Recently, in [18, 19] a multilayer SIW integrated planar horn antenna is proposed based on stacked sections. The stepped technique has been used in different frequency ranges [18–20, 31]. To our best knowledge, the stepped technique is used for the first time in E-band. The very low losses in the mm-Waves band of horn antennas place them as ideal candidates to develop new promising small-cell flat structures. The structure is jointly optimized on CST Microwave Studio Software (version 2013) [39] and Empire (version Empire XPU 7.02) [40] for the optimization of openings and radiation. A reduction about 25% of the total height (from 8.9 mm reduced to 6.6 mm) is achieved in comparison to a "classical" rectangular shape horn element with the same performances. In order to keep the same inter-element spacing d, the surface $A_e = 3.4 \times 3.4\,\text{mm}^2$ remains identical. As mentioned before, the rectangular section of the waveguide at the entrance of the SHE has a smaller section ($a \times b = 2.3 \times 1.0$ in mm, Fig. 1) than that of the WR12 standard E-band waveguide ($a' \times b' = 3.09 \times 1.54$ in mm). This section has been optimized to present a large bandwidth and a maximum energy transfer ($|S_{11}| < -35$ dB and $\text{MS}_{21} = 0$ dB from 70- to 86-GHz). The final optimized SHE dimensions are given in Fig. 1.

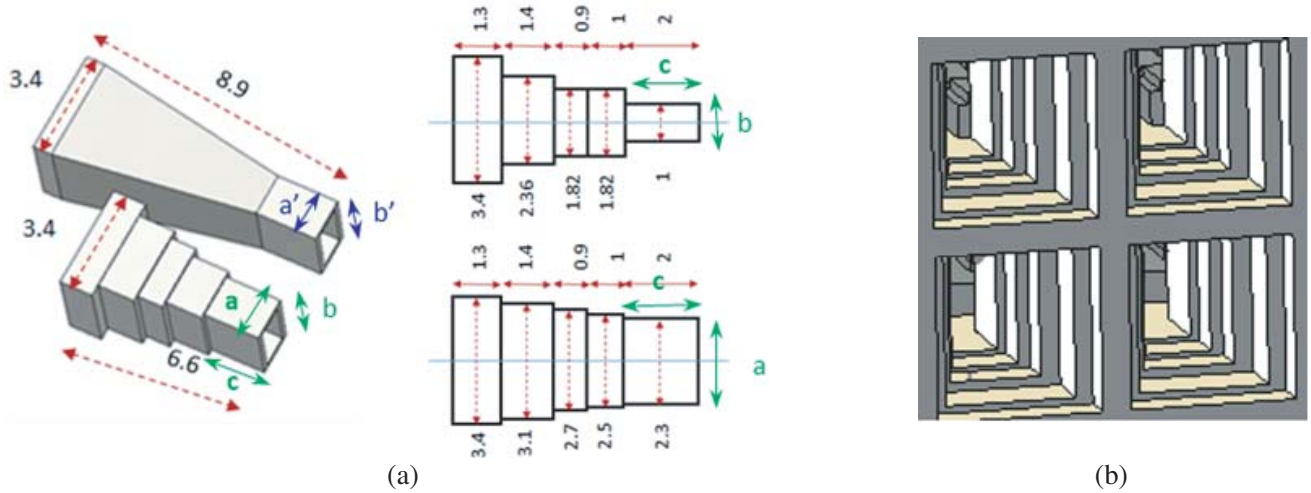

(a) (b)

Figure 1. (a) Comparison of the dimensions of the proposed compact stepped horn element (SHE) and the "classical horn" element with the same aperture surface and performances. Final dimensions (in mm) of the SHE: $a = 2.3$, $b = 1$, of the WR12: $a' = 3.0988$, $b' = 1.5494$, (b) CST Model (View) of the simulated array network.

Figure 2. Prototype of the Design SHE antenna (radiating element and the RWG transition between the horn and a WR12 rectangular waveguide section). The dimensions of all the rectangular sections are given in Fig. 1.

Layer-by-layer micromachining with high manufacturing tolerances (precision better than 50 µm) was used to fabricate the horn antenna composed of the SHE and the waveguide transitions to the WR12 WG input port. The realized prototype of the SHE is shown in Fig. 2. The measured and simulated reflection coefficients of SHE are depicted by Fig. 3. The elementary antenna offers a good impedance matching with a measured return loss above 20 dB (magnitude of the reflection coefficient; $|S_{11}| < -20$ dB) over the full frequency band (from 71 GHz to 86 GHz). The measured and simulated reflection coefficients (magnitude S_{11} (dB)) are in good agreement.

Radiation patterns measurements are performed in an indoor anechoic chamber facility. Both transmitting and receiving antennas were placed along the broadside direction. The mast with the antenna under test (AUT) ensures a horizontal rotation from $-180°$ to $180°$ with $0.1°$ step, monitored by an embedded ANT32 Soft from CT Systems [41]. The measured radiation diagrams are compared to those obtained by the electromagnetic simulations using two electromagnetic softwares, the CST MWS [39] and Empire software [40]. Fig. 4 shows an example of simulated and measured radiation diagrams at 86 GHz, both in the E- and H-planes, respectively ($Phi = 0°$ and $Phi = 90°$). At 86 GHz, the aperture angle (at -3 dB) is of $\sim 65°$ in the E-plane and $\sim 57°$ in the H-plane. The measured gain of the antenna is between 8.6 dB and 9.6 dB over most of the antenna bandwidth. Good

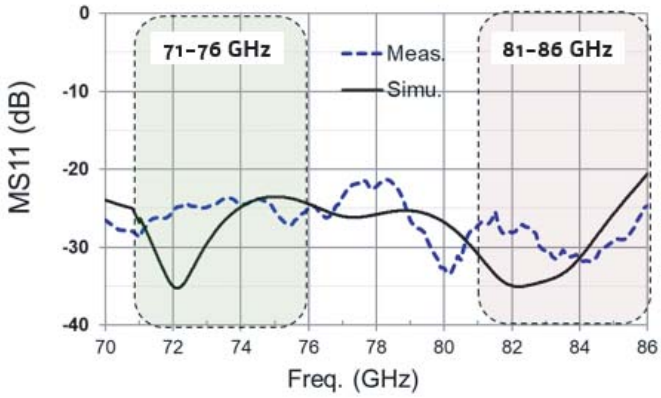

Figure 3. Comparison between the measured and simulated magnitude of the reflected coefficient; $|S_{11}|$ (dB), of the designed SHE antenna.

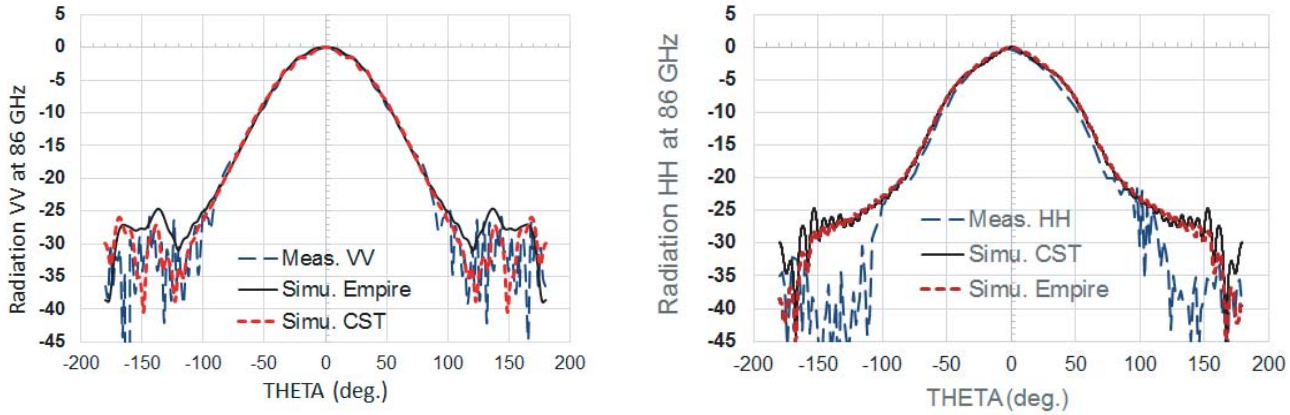

Figure 4. Radiation patterns of the elementary SHE antenna. Measured and simulated results at 86 GHz. (a) E-plane, and (b) H-Plane.

agreement is obtained between measurement and simulations results (Fig. 4). In order to verify the order of magnitude of the antenna's gain, Equation (A1) (see appendix) may be used to approximate the maximum available directivity, assuming an aperture efficiency equal to 1. Equation (A1) is rather valid for antennas with larger surface. Table 1 summarizes the measured performances (gain and aperture angle at -3 dB) of the elementary antenna (SHE), at different frequencies in the E-band (71 to 86 GHz) in comparison with the calculated values using Equation (A1).

Table 1. Measured, Simulated and calculated (Equation (A1)) performances of the elementary stepped horn antenna (SHE).

Frequency	Gain (dB)	-3 dB Aperture angle (Deg.) (E-Plane, H-Plane)	Max directivity (dB), Equation (A1) (Appendix)
71 GHz	8.6	(63.5°, 67.5°)	9
76 GHz	8.95	(67.5°, 62.5°)	9.6
81 GHz	9.2	(67.4°, 61.5°)	10
86 GHz	9.6	(64.7°, 57.5°)	10.7

3. DESIGN OF THE ANTENNA ARRAY

3.1. Network Feeding Architecture

Figure 5 depicts a part of the schematic bloc of the feeding-network. It is composed of sophisticated mixed horizontal and vertical feeding portions (Fig. 5(a)). The horizontal feeding potion is composed of 3 dB equal power dividers designed using ridged waveguide (RWG) technique. This technique is usually used in order to increase the frequency bandwidth meanwhile reducing the WG dimensions. The vertical portion allows linking the planar feeding portion to the SHE radiating antenna. Compact broadband waveguide polarization rotation component (polarizer or twister 90°) with a total height of 1.6 mm is designed based on multi-section bow-tie shape structure [32–36]. It can be rotated in order to resolve the out of phase shift which occurs during changing axis. Figs. 5(b)–(c) illustrate the simulated Electrical field (E) at the two output ports of the power divider. Without the polarizer, one can see that the E vectors ($E2$ and $E3$) are out of phase (Fig. 5(b)). With the phase shift rotator (polarizer 90°), the two output E fields, $E2$ and $E3$, are now in phase (Fig. 5(c)). Fig. 6 shows the complete vertical part of the feeding network and a radiated element (all the dimensions in the legend are in mm). It consists of a SHE antenna, a twister device or a polarizer, a RWG transition, and a WR12 rectangular input wave port. The implementation — antenna array and its complete feed network — using waveguide techniques is an original contribution for the E band where the dimensions and wavelengths (λ) are so small ($\lambda_0 = 3.4$ mm at 86 GHz).

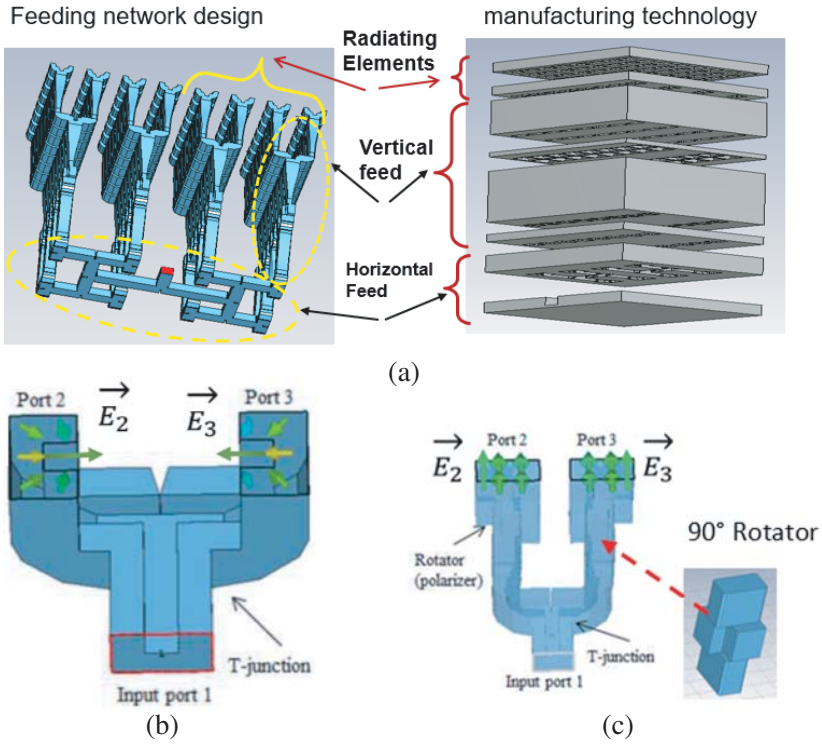

Figure 5. Feeding network in waveguide technology. (a) Proposed architecture with the horizontal and vertical parts including respectively the 3 dB power divider, and the polarization rotation component (90°) and transitions. (b) Design of the RWG power divider, and (c) Added compact polarizers (shift phase) to obtain in phase output **E** fields (at the output ports E2 and E3). The RWG section dimensions are $a \times b = 2.3 \times 1\,\text{mm}^2$.

3.2. Design of Antenna-Array of 32 × 32 Elements

A flat antenna array of 32 × 32 horn elements antenna with the whole feeding network is studied and fully optimized using both CST-MWS and Empire electromagnetic software. The analytical expression

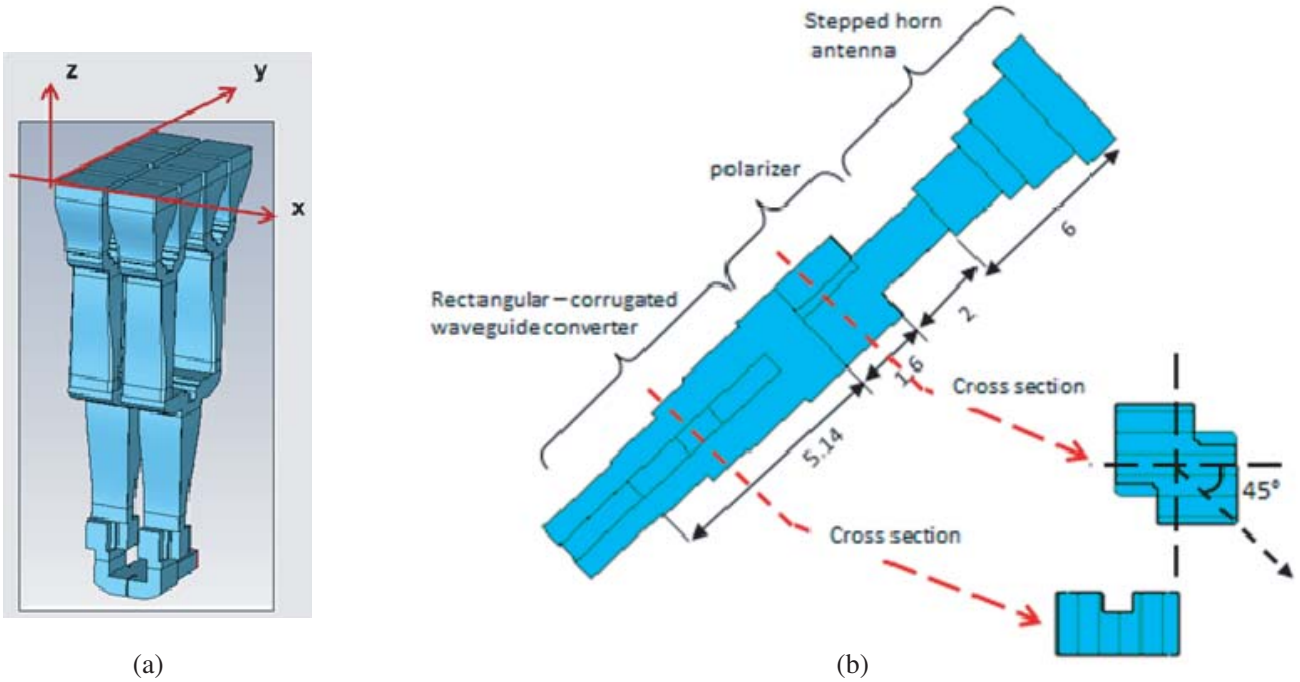

(a) (b)

Figure 6. (a) Vertical part of the feeding network (ridged waveguide transition + polarizer) and (b) Complete structure of the designed stepped horn antenna (with main dimensions in mm).

of the total radiated field $\mathbf{E_{tot}}(\boldsymbol{\theta})$ of the array antenna is given by Equations (A3) to (A5) given in the Appendix A. Fig. 7(a) shows the CST model of the antenna array composed of 32×32-SHE elements. To avoid the generation of multiple beams grating lobes the elements are spaced by $d < \lambda_0$ using Equation (A6) (given in Appendix A) with λ_0 calculated at highest operating frequency ($f_0 = 86\,\text{GHz}$) [8, 26]. The number $N \times N = 32\times32$ of radiating elements generates a pencil beam pattern in the main direction ($\theta_0 = 0°$) with a half-power beamwidth ($-3\,\text{dB}$ BW°) of $\text{BW}_{-3\text{dB}}<100/\text{N} \sim 3°$. Figs. 7(b) and 7(c) show the radiation diagrams of the 32×32 antenna array simulated in the E-, H-, and Secant-diagonal D-planes (respectively $Phi = 0°$, 90°, and 45°) for the limit frequencies of the E-band spectrum, 71- and 86-GHz, respectively. The antenna is fed with equal weight amplitude (uniformly excited using the same source). Note that in the simulated results, one can observe the classic behaviour of square antennas, with the appearance of secondary lobes in the E- and H-planes and their quasi-absence in the secant D-plane. Fig. 7(d) shows the simulated reflection coefficient, $|S_{11}|$, (dB) of the antenna array. The antenna is well matched over the entire E-band domain with an $|S_{11}|$ (dB) $\leq -20\,\text{dB}$. As shown by Figs. 7(b)–(c), the minimum directivity (main lobe) is $\sim 38\,\text{dB}$ at 71 GHz (and 40 dB at 86 GHz) which is in agreement with the calculated value given by Equation (A3) (given in Appendix A). In the D-plane, the sidelobe levels (minor lobes) are very low ($> 26\,\text{dB}$ below the main lobe for the two paired bands (71–76 GHz and 81–86 GHz).

Tables 2(a) and 2(b) summarize the simulated performances of the 32×32 antenna array excited uniformly in terms of directivity, realized gain, aperture angle ($-3\,\text{dB}$ BW°), and first sidelobe level in the E-band spectrum (71 to 86 GHz). To further decrease the level of the secondary lobes (SLL) and ovoid Electromagnetic Interference (EMI) problems, a nonuniform feeding antenna (weight coefficients) is commonly used [42]. It is also possible to optimize the inter-element distances for a nonuniform 2D layout [42–44]. The application of these optimization techniques allows the network antennas to meet the ETSI criteria (class 3) [27].

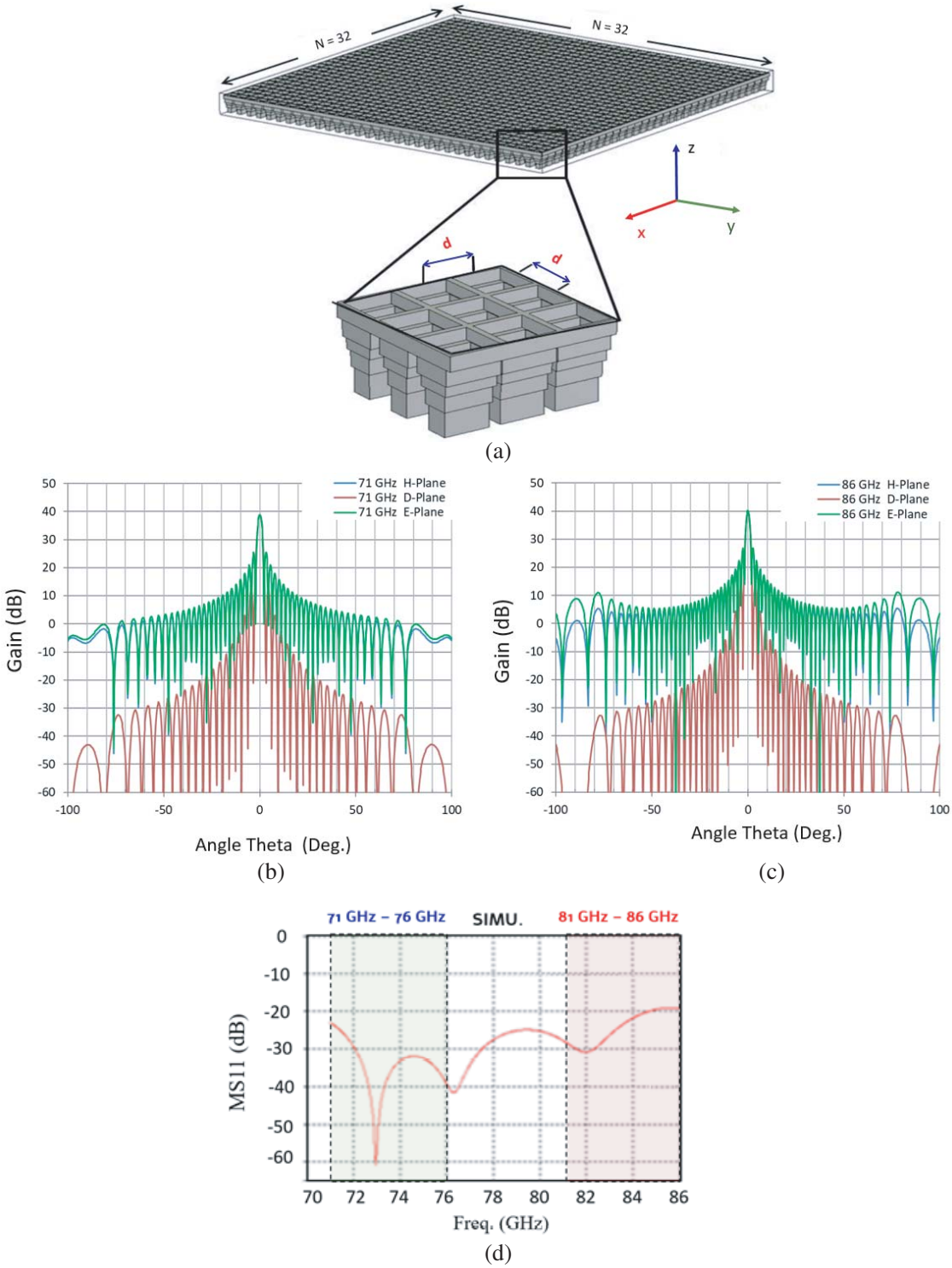

Figure 7. Performances of the 32×32 antenna array. (a) Radiating part of the antenna array, (b) and (c) Simulated (CST) radiation diagrams of in the plane E-, H-, and D-Planes (respectively Theta $= 0°$, $90°$ and slant at $45°$) for the edge frequencies 71 and 86 GHz of the E-band spectrum. The network antenna is supplied uniformly with identical amplitude on all sources, and d) Magnitude of the simulated reflection coefficient ($|S_{11}|$ (dB) of the antenna array.

Table 2. (a) Simulated performances of the 32×32 array antenna $d = 3.4\,\text{mm}$: D-plane. (b) Simulated performances of the 32×32 array antenna $d = 3.4\,\text{mm}$: E- and H-planes.

Frequency	Directivity (dB) at boresight	***D-plane*** - First Side lobe level (dBc), - Beamwidth (BW°)	
71 GHz	39.1	-26.7	2.5°
76 GHz	39.7	-26.5	1.9°
81 GHz	40.3	-26.5	1.8°
86 GHz	40.7	-26.8	1.7°

Frequency	Cut-Plane	Gain (dB) at boresight	First Side lobe level (dBc), Beamwidth (BW°)	
71 GHz	H-Plane	38.76	-13.3	1.8
71 GHz	E-Plane	38.76	-13.3	1.9°
71 GHz	D-Plane	38.76	-26.5	1.8°
86 GHz	H-Plane	40.22	-13.4	1.7°
86 GHz	E-Plane	40.22	-13.4	1.6°
86 GHz	D-Plane	40.22	-26.5	1.62°

3.3. C 4×4 Sub-Array Antenna: Design and Simulation Results

We present here an experimental validation with a subarray of 4×4 horn elements (see details in Section 4). The numerical model of the 4×4 antenna array on CST MWS finely describes the waveguide device composed of the SHE, WG transitions, twisters, 3 dB power dividers, ...

The simulated reflection coefficient S_{11} (dB) is presented in Fig. 8. A good matching impedance ($S_{11}(\text{dB}) < -10\,\text{dB}$) is performed over the whole E-band. The Far-Field radiation patterns are simulated for the main polarization (Co-Pol) and the crossed polarization (X-Pol) in three cut-planes: E-plane (Phi = 0°), H-plane (Phi = 90°), and diagonal plane (Phi = 45°). From Fig. 9(a) through Fig. 9(c) the realized gain is presented for different frequencies; 71, 73.5, 76, 81, and 86 GHz of the E-band. The design antenna array radiates in the normal axis (broadside, $\theta = 0°$) with a symmetrical diagram, high gain, very low crossed polarisation radiation, low sidelobe levels, and low backward radiation. The SLL is $< -15\,\text{dB}$ below the level of the main lobe in the E-plane (Fig. 9(a)), $< -13\,\text{dB}$ in the H-plane (Fig. 9(b)), and $<-30\,\text{dB}$ in the D-plane (Fig. 9(c)). The crossed polarization is at least $-40\,\text{dB}$ below the main lobe level in the E-plane (Fig. 9(a)), under $-40\,\text{dB}$ in the H-plane (Fig. 9(b)), and $-30\,\text{dB}$ in the D-plane (Fig. 9(c)). The simulated radiation efficiency of the antenna array is above 77.5% within the bandwidth of the antenna, from 71 GHz to 86 GHz. The realized gain is unchanged in frequency with almost stable value of 22 dB.

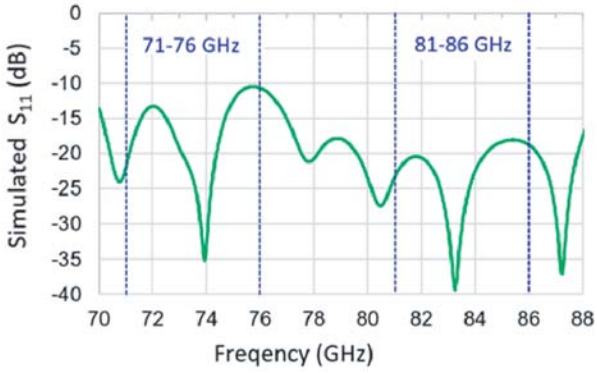

Figure 8. Magnitude of the simulated reflection coefficient of the 4×4 antenna array.

4. EXPERIMENTAL CHARACTERIZATION 4×4 ANTENNA

4.1. Prototype 4×4 Antenna Array

In order to satisfy tolerances required by the electric discharge machining (EDM) manufacturing process, which needs a precision better than 0.05 mm, the antenna sub-array is divided into three main blocs (or layers) as depicted in Fig. 10. Layer 1 contains the $N \times N$-SHE radiating elements and transitions to

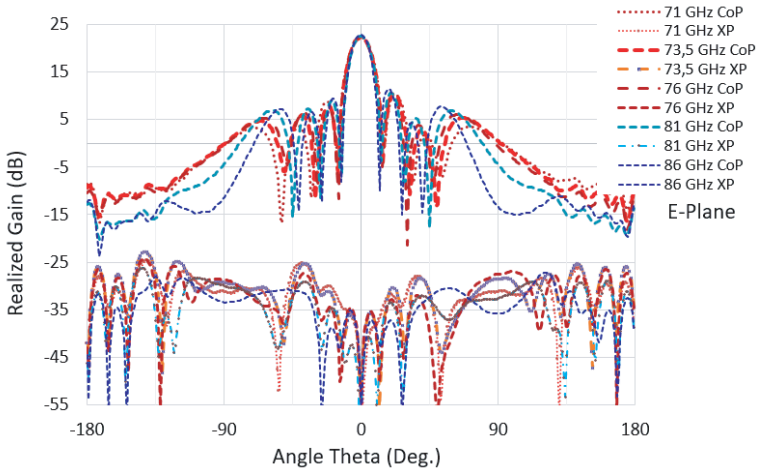

(a)

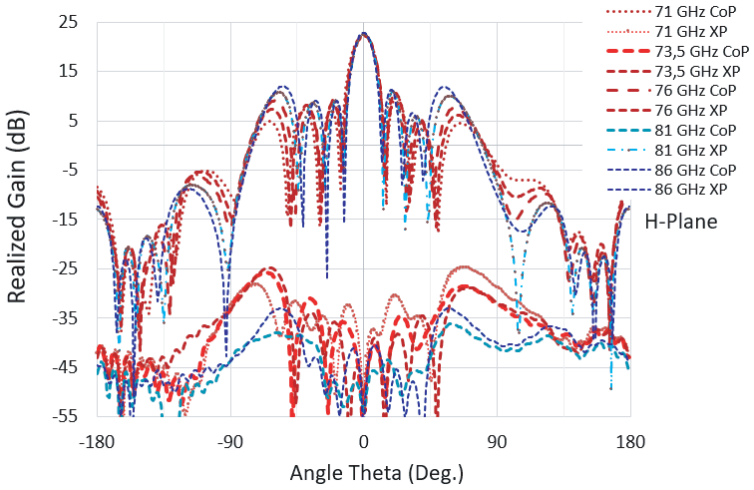

(b)

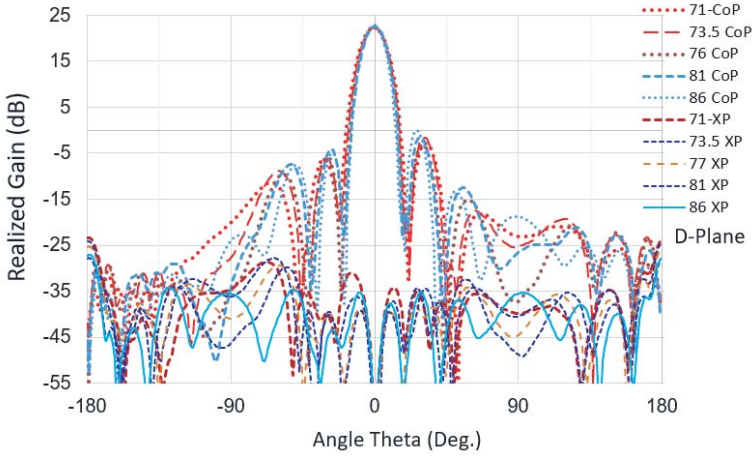

(c)

Figure 9. Simulated radiation patterns of the 4×4 antenna array. Realized gain in Cartesian forms at the principal and crossed polarizations for different frequencies of the E-Band. (a) in the E-Plane (Phi $= 0°$), (b) In the H-Plane (Phi $= 90°$) and (c) In the D-Plane (Phi $= 45°$).

the polarizer (90° twisters). Layer 2 contains the polarizers and all vertical RWG transition elements. Layer 3 contains the horizontal WG feeding network (powers-dividers, adaptors, ...). An additional WG transition portion is placed at the entrance to connect the standard WR12 port to the WG feeding network (Fig. 1). A prototype 4×4 antenna subarray was realized and fully characterized in the E-band. Fig. 11 shows photographs of the 4×4 manufactured antenna at different cut-views. The total dimensions are about $13.6 \times 13.6 \times 18\,\text{mm}^3$ (width, height, thickness). Fig. 11(a) is a global view of the realized antenna. Fig. 11(b) and Fig. 11(c) show the different layers (schematically described in Fig. 10) and the complete WG power-feeding network. The EDM method is very appropriate here with accurate angles cutting and mechanical tolerances.

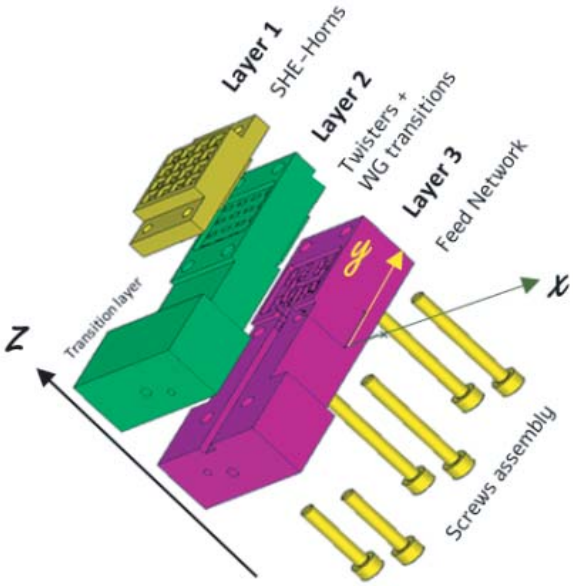

Figure 10. Electric discharge machining (EDM) manufacturing process: the proposed antenna composed of three layers is assembled by six screws located along the antenna, two on the side of the WR12 input port, two in the center and the last at the ends of the radiating part of the antenna.

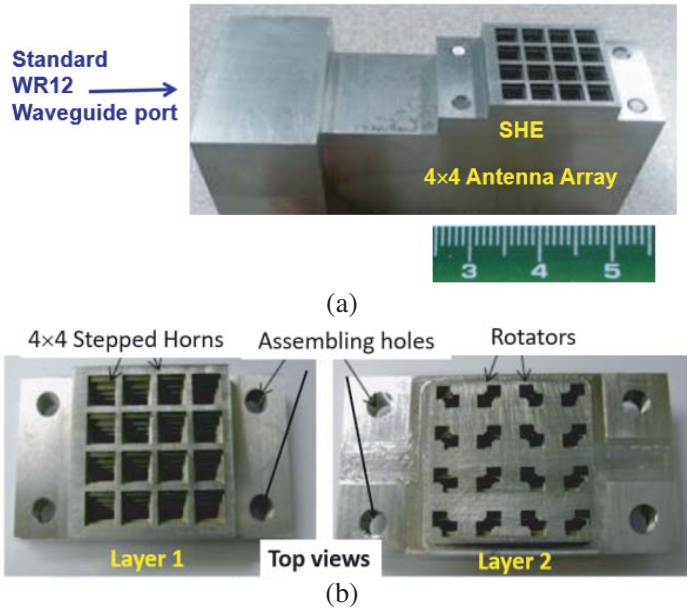

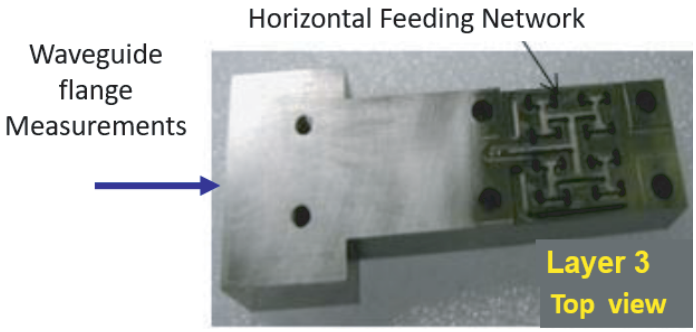

(c)

Figure 11. Photographs of the fabricated 4×4 prototype E-band antenna array (different views). (a) Overview of the antenna and its WR12 input port, (b) "Layer1" top view (left) and "Layer 2" top view, with the footprint of the bow-tie shape polarizers, and (c) "Layer 3" Top view. We see also the transition between the WR12 standard and the horizontal RWG feeding network (right).

4.2. Measurement Results and Comparison to the Simulations

The 4×4 antenna array is characterized in an anechoic chamber of RFS-Trignac. The radiation patterns are measured in two major E- and H-cut-planes (respectively Phi-0°, and Phi = 90°) over the whole 71–86 GHz frequency band. Fig. 12 presents the normalized curves of the measured radiation diagrams, respectively in E-plane (Fig. 12(a)) and H-plane (Fig. 12(b)) for five frequencies of interest; 71, 73.5, 76, 81, and 86 GHz. The radiation pattern measured in the E plane shows a slight asymmetry at 71 GHz. The main lobe and side lobe are unresolved (at negative theta angle). This phenomenon disappears when the frequency is increased. In the H-plane behaviour is almost stable over the whole frequency band (Fig. 12(b)). The measured realized gain is ≥ 19.6 dB, and the half power beam widths (BW) is $\leq 15°$. The measured back radiations are very low (< -50 dB), about 10 to 15 dB below the simulated levels (shown Figs. 9(a), (b)).

Figure 13 represents the superimposed simulated and measured reflection coefficients of the overall antenna. The measured S_{11} (dB) is better than -12 dB for the frequency range of 71–76 GHz and -15 dB for the 81–86 GHz band. The antenna is well matched over the entire E band, although there is

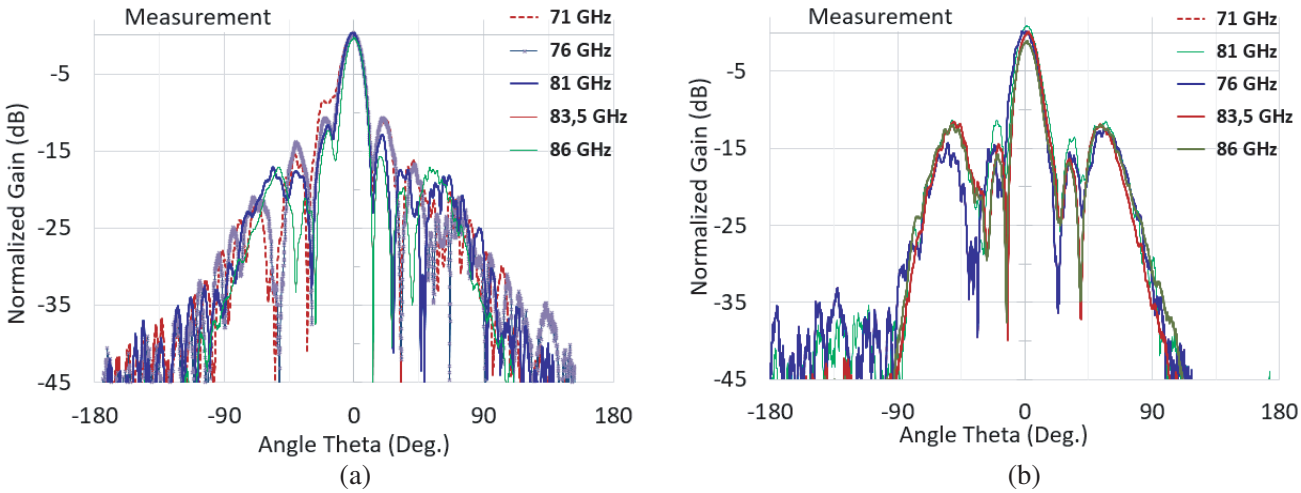

(a) (b)

Figure 12. Measured far field radiation patterns. (Cartesian forms) in the E-band spectrum from 71 GHz to 86 GHz. Normalized curves. (a) in the E-Plane (Phi = 0°), and (b) In the H-Plane (Phi = 90°).

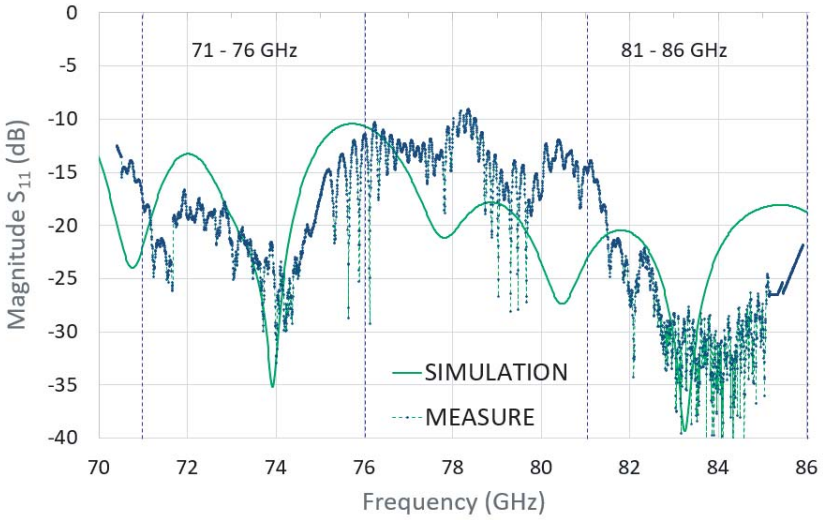

Figure 13. Comparison of the measured and simulated magnitude of the reflection coefficient (S_{11} parameter) versus frequency of the 4×4 Sub array antenna.

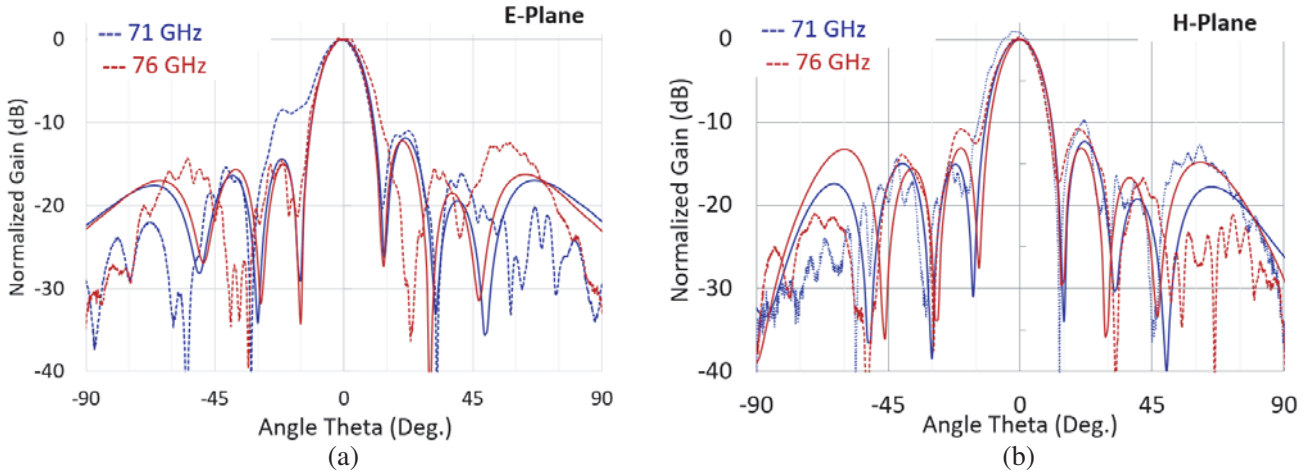

Figure 14. Comparison of the measured and simulated Far Field radiation diagrams (Cartesian forms) in the 71–76 GHz band. Normalized curves in the (a) E-Plane (Phi = 0°) and (b) H-Plane (Phi = 90°).

a rightward shift in the S_{11} measurement curve in the 71–76 GHz band. We can interpret the differences between the measurement and simulations with possible misalignment when assembling the three layers of the antenna which may have, as consequence, the shift of the spectrum and a bad adaptation to the limiting frequencies, in particular of the first band (71 and 76 GHz). The second band is very well matched. The measured bandwidth ($S_{11} < -10$ dB) of the antenna is 5 GHz for each band corresponding to relative bandwidths of 6.8% and 5.9%, respectively.

Figure 14 shows simulated and measured E- and H-plane radiation patterns of the proposed 4×4 horn antenna at two different frequencies (71 and 76 GHz). All the results are normalized to the maximum value. Fig. 15 gives the same normalized radiation patterns for the second band at 81 and 86 GHz. The slight difference observed between the simulation and measurement of the antenna array can be attributed to the tolerances of the manufacturing process and/or to the possible misalignment during the assembly of the three layers of the antenna.

Good agreements are obtained for the directivity, SLL, and beamwidth which are quite identical in the E- and H-planes. Table 3 summarizes the measured 4×4 sub antenna array in terms of gain,

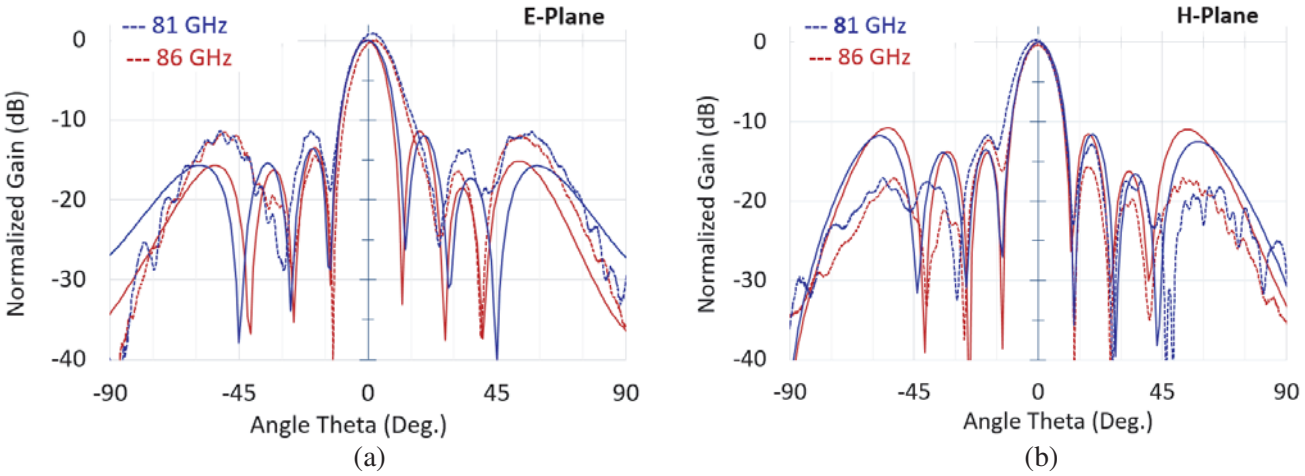

Figure 15. Comparison of the measured and simulated Far Field radiation diagrams (Cartesian forms) in the 81–86 GHz band. Normalized curves in the (a) E-Plane (Phi = 0°) and (b) H-Plane (Phi = 90°).

Table 3. Measured performances of the 4×4 array antenna.

Frequency	Gain (dBi)	First Side Lobe Level (dB),	
		−3 dB Aperture angle (Deg.)	
71 GHz	19.7	−11	13.2°
76 GHz	19.9	−12	12.9°
81 GHz	20.7	−13.2	13.2°
86 GHz	20.9	−16.5	16.5°

aperture angle (at −3 dB), and the first side lobe level in the E-band (71 to 86 GHz). The cross-polarization level is measured also for different frequencies (results not shown in this paper) and fit well to the simulation results (of Fig. 12).

5. CONCLUSION

In this paper, a highly directive waveguide small-cell flat antenna array (32×32 elements) with compact sizes ($100 \times 100 \times 25\,\text{mm}^3$) and a complete feeding network is presented. Featuring a high directivity, a wide bandwidth covering the E-band, a very low back radiation, a very low cross-polarization, and quite low side lobes, the antenna is dedicated to high-bit rate point-to-point communications in E-band. A new compact stepped horn antenna, SHE (6.6 mm height and $3.4 \times 3.4\,\text{mm}^2$ aperture surface) is designed, manufactured, and characterized. Good agreements are obtained with the electromagnetic CST MWS and Empire models. Ridged waveguide transitions, 3 dB-power dividers, and bow-tie multi-section waveguide polarizer rotator (±90°) are designed and experimentally characterized. They exhibit a broadband frequency response, low insertion loss, and low cut-frequency ($\leq$ 55 GHz) much better than the standard waveguide in the E-bandwidth. A 4×4-elements array and the waveguide power-feeding network are simulated, manufactured, and measured. The measured gain is higher than 19.7 dB at 71 GHz and 20.9 dB at 86 GHz, and correspondingly the antenna efficiency is larger than 77.5% over the whole E-band spectrum. The help of a 3D printer paves the way for many potential applications implementing low cost solutions and mass production at mm-wavelengths. Our results constitute a further step towards the realization of compact, broadband, very directive antennas for high speed wireless point-to-point communications and many applications such 5G and anti-collision radars for autonomous vehicles.

ACKNOWLEDGMENT

The authors wish to express our gratitude towards RFS Trignac-France for the manufacturing and the test measurements facilities. Thanks to System@Tic Paris-Region for their financial supports during the Elhan project for High Speed Digital Link in E-Band carried by Alcatel-Lucent. Thank you to Mr. Gérard Collignon for the fruitful scientific discussions, valuable advice and partnership on the scientific projects.

APPENDIX A.

$$D = 4\pi \frac{A_e}{\lambda^2} \tag{A1}$$

$$D(\mathrm{dB}) = 10 \times \log_{10}(D) \tag{A2}$$

$$E_{tot}(\theta) = \frac{K}{r} e^{-ikr} f(\theta) \sum_{k=0}^{N} a_k \times e^{i\psi_k} \tag{A3}$$

$$AF = \sum_{k=0}^{N} a_k \times \exp(i\psi_k) \tag{A4}$$

$$\psi_k = \varphi_k + \frac{2\pi}{\lambda} d_k \cos(\theta_k) \tag{A5}$$

$$d < \frac{\lambda_0}{1 + |\sin(\theta_k)|} \tag{A6}$$

where $f(\theta)$ is the radiation pattern of a basic element (SHE) of the array antenna; AF is the array factor; θ and ϕ are the angles of a spherical-coordinate system. $d_k = d$ is the inter-element distance, a_k the complex amplitude distribution, Ψ_k the phase variations, and θ_k the beam pointing direction (scan angle or elevation angle). $k = 2\pi/\lambda$ is the wavenumber and λ the free space wavelength calculated at the desired frequency.

The array elements are spaced by $d < \lambda_{86\,GHz}$ using Equation (A6) where λ_0 is calculated at the highest operating frequency ($f_0 = 86\,\mathrm{GHz}$).

- 86 GHz, $\theta_k = 0°$ $\quad d \leq \lambda_0 = 3.48\,\mathrm{mm}$
- 86 GHz, $\theta_k = 90°$ $\quad d \leq \lambda_0/2 = 1.74\,\mathrm{mm}$

REFERENCES

1. Dyadyuk, V., Y. J. Guo, and J. D. Bunton, "Multi-gigabit wireless communication technology in the E-band," *1st International Conference on Wireless Communication, Vehicular Technology, Information Theory and Aerospace & Electronics Systems Technology, Wireless VITAE 2009*, 2009.
2. Niu, Y., Y. Li, D. Jin, et al., "A survey of millimeter wave communications (mmWave) for 5G: opportunities and challenges," *Wireless Networks*, Vol. 21, No. 8, 2657–2676, 2015.
3. Liu, J., A. Vosoogh, A. U. Zaman, et al., "A slot array antenna with single-layered corporate-feed based on ridge gap waveguide in the 60 GHz band," *IEEE Transactions on Antennas and Propagation*, Vol. 67, No. 3, 1650–1658, 2018.
4. Vosoogh, A., -S. Kildal, and V. Vassilev, "Wideband and high-gain corporate-fed gap waveguide slot array antenna with ETSI class II radiation pattern in V-band," *IEEE Transactions on Antennas and Propagation*, Vol. 65, No. 4, 1823–1831, 2016.
5. Liu, J. Liu, W. Hu, et al., "Hollow waveguide 32×32-slot array antenna covering 71–86 GHz band by the technology of a polyetherimide fabrication," *IEEE Antennas and Wireless Propagation Letters*, Vol. 17, No. 9, 1635–1638, 2018.

6. Gallee, F., G. Landrac, and M. M. Ney, "Artificial lens for third-generation automotive radar antenna at millimetre-wave frequencies," *IEE Proceedings-Microwaves, Antennas and Propagation*, Vol. 150, No. 6, 470–476, 2003.
7. Vosoogh, A., et al., "Compact integrated full-duplex gap waveguide-based radio front end for multi-Gbit/s point-to-point backhaul links at E-band," *IEEE Transactions on Microwave Theory and Techniques*, Vol. 67, No. 9, 3783–3797, 2019.
8. Wang, L., et al., "Wideband and dual-band high-gain substrate integrated antenna array for E-band multi-gigahertz capacity wireless communication systems," *IEEE Transactions on Antennas and Propagation*, Vol. 62, No. 9, 4602–4611, 2014.
9. Mehrpouyan, H., et al., "Improving bandwidth efficiency in E-band communication systems," *IEEE Communications Magazine*, Vol. 52, No. 3, 121–128, 2014.
10. Schäfer, F., F. Gallee, G. Landrac, and M. Ney, "Optimum reflector shapes for anti-collision radar at 76 GHz," *Microwave and Optical Technology Letters*, Vol. 24, No. 6, 400–404, 2000.
11. Yang, J., I. Papageorgiou, A. Derneryd, and L. Manholm, "An E-band cylindrical reflector antenna for wireless communication systems," *7th European Conference on Antennas and Propagation, EuCAP 2013*, Gothenburg, Sweden, Apr. 8–12, 2013.
12. Artemenko, A., A. Mozharovskiy, A. Maltsev, R. Maslennikov, A. Sevastyanov, and V. Ssorin, "Experimental characterization of E-band two-dimensional electronically beam-steerable integrated lens antennas," *IEEE Antennas and Wireless Propagation Letters*, Vol. 12, 1188–1191, 2013.
13. Al-Nuaimi, M., K. Taher, and W. Hong, "Discrete dielectric reflectarray and lens for E-band with different feed," *IEEE Antennas and Wireless Propagation Letters*, Vol. 13, 947–950, 2014.
14. Al-Nuaimi, Mu. K. T., W. Hong, and Y. Zhang, "Design of high-directivity compact-size conical horn lens antenna," *IEEE Antennas and Wireless Propagation Letters*, Vol. 13, 467–470, 2014.
15. Pan, B., et al., "A 60-GHz CPW-fed high-gain and broadband integrated horn antenna," *IEEE Transactions on Antennas and Propagation*, Vol. 57, No. 4, 1050–1056, 2009.
16. Ghassemi, N. and K. Wu, "Planar high-gain dielectric-loaded antipodal linearly tapered slot antenna for E- and W -Band gigabyte point-to-point wireless services," *IEEE Transactions on Antennas and Propagation* Vol. 61, No. 4, 1747–1755, 2013.
17. Ghassemi, N. and K. Wu, "High-efficient patch antenna array for E-band gigabyte point-to-point wireless services," *IEEE Antennas and Wireless Propagation Letters*, Vol. 11, 1261–1264, 2012.
18. Ghassemi, N. and K. Wu, "Millimeter-wave integrated pyramidal horn antenna made of multilayer printed circuit board (PCB) process," *IEEE Transactions on Antennas and Propagation*, Vol. 60, No. 9, 4432–4435, 2012.
19. Deslandes, D. and K. Wu, "Integrated microstrip and rectangular waveguide in planar form," *IEEE Microwave and Wireless Components Letters*, Vol. 11, No. 2, 68–70, 2001.
20. Encinar, J. and J. Rebollar, "A hybrid technique for analyzing corrugated and noncorrugated rectangular horns," *IEEE Transactions on Antennas and Propagation*, Vol. 34, No. 8, 961–968, 1986.
21. Zhang, M., J. Hirokawa, and M. Ando, "An E-band partially corporate feed uniform slot array with laminated quasi double-layer waveguide and virtual PMC terminations," *IEEE Transactions on Antennas and Propagation*, Vol. 59, No. 5, 1521–1527, 2011.
22. Gueye, M. B., H. H. Ouslimani, S. N. Burokur, A. Priou, Y. Letestu, and A. Le Bayon, "Antenna array for point-to-point communication in E-band frequency range," *IEEE International Symposium Antennas and Propagation (APSURSI)*, 2077–2079, Jul. 2011.
23. FanHong, M., H. H. Ouslimani, and M. B. Gueye, "Experimental study of 80 GHz Fabry-Pérot cavity antenna based on dual-layer partially reflected surface," *Electronics Letters*, Vol. 51, No. 22, 1730–1732, 2015.
24. Ouslimani, H. H. and F. Meng, "Design of large-band highly directive antenna in the millimeter waves range at 80 GHz," *2019 IEEE International Symposium on Antennas and Propagation and URSI Radio Science Meeting, IEEE*, 1097–1098, 2019.

25. Chacko, B., G. Augustin, and T. A. Denidni, "FPC antennas: C-band point-to-point communication systems," *IEEE Antennas and Propagation Magazine*, Vol. 58, No. 1, 56–64, 2016.
26. Balanis, C. A., *Antenna Theory: Analysis and Design*, John wiley & sons, 2016.
27. ETSI (European Telecommunications Standards Institute), **European Standard** EN 302 217-4-2, "Fixed radio systems; Characteristics and requirements for point-to-point equipment and antennas; Part 4-2: Antennas; Harmonized EN covering the essential requirements of article 3.2 of R&TTE directive," 2–35, 2010, http://www.etsi.org and https://www.google.com/search?hl=fr&q=Final+draft+ETSI+EN+302+217-4-2+V1.4.1+(2008-11).
28. HPCPE-80, "High performance parabolic reflector antenna, single-polarized, 71–86 GHz," https://www.radiowaves.com/en/product/hpcpe-80 and https://www.radiowaves.com/en/product/hplp2-80. 2020.
29. Migliaccio, C., B. D. Nguyen, C. Pichot, et al., "Fresnel reflector antennas for mm-Wave helicopter obstacle detection radar," *IEEE 2006 First European Conference on Antennas and Propagation*, 1–5, 2006.
30. Gomez, J., Tayebi, A., J. de Lucas, et al., "Metal-only Fresnel zone plate antenna for millimetre-wave frequency bands," *IET Microwaves, Antennas & Propagation*, Vol. 8, No. 6, 445–450, 2014.
31. Wriedt, T., et al., "Rigorous hybrid field theoretic design of stepped rectangular waveguide mode converters including the horn transitions into half-space," *IEEE Transactions on Antennas and Propagation*, Vol. 37, No. 6, 780–790, 1989.
32. Jorge, A. R.-C., R. M.-G. José, and M. R. Jesús, "Multi-section bow-tie steps for full-band waveguide polarization rotation," *IEEE Microwave and Wireless Components Letters*, Vol. 20, No. 7, 375–377, Jul. 2010.
33. Chen, L., A. Arsenovic, J. R. Stanec, T. J. Reck, A. W. Lichtenberger, R. M. Weikle, II, and N. S. Barker, "A micromachined terahertz waveguide 90 twist," *IEEE Microwave and Wireless Components Letters*, Vol. 21, No. 5, 234–236, May 2011.
34. Kirilenko, A., D. Y. Kulik, and L. A. Rud, "Compact 90 twist formed by a double-corner-cut square waveguide section," *IEEE Trans. Microw. Theory Tech.*, Vol. 56, No. 7, 1633–1637, Jul. 2008.
35. Kirilenko, A., D. Y. Kulik, and L. A. Rud, "Compact broadband 90 twist based on square waveguide section with two stepped corner ridges," *Microwave Opt. Technol. Lett.*, Vol. 51, No. 3, 851–854, Mar. 2009.
36. Beis, K. and U. Rosenberg, "Waveguide Twist," U.S. Patent 6 879 221 B2, Apr. 12, 2005.
37. Zhang, B., et al., "Metallic, 3D-printed, K-band-stepped, double-ridged square horn antennas," *Applied Sciences*, Vol. 8, No. 1, 33, 2017.
38. Zhang, B., Y.-X. Guo, H. Zirath, et al., "Investigation on 3-D-printing technologies for millimeter-wave and terahertz applications," *Proceedings of the IEEE*, Vol. 105, No. 4, 723–736, 2017.
39. Franz Hirtenfelder, "Effective antenna simulations using CST microwave studio®," Apr. 2007, DOI: 10.1109/INICA.2007.4353972, Source: IEEE Xplore https://www.3ds.com/fr.
40. EMPIRE XPU, http://www.empire.de.
41. ANT32, CT Systems, https://www.ctsystemes.com.
42. Recioui, A., "Sidelobe level reduction in linear array pattern synthesis using particle swarm optimization," *Journal of Optimization Theory and Applications*, Vol. 153, No. 2, 497–512, 2012.
43. Hodjat, F. and S. et Hovanessian, "Nonuniformly spaced linear and planar array antennas for sidelobe reduction," *IEEE Transactions on Antennas and Propagation*, Vol. 26, No. 2, 198–204, 1978.
44. Oraizi, H. and M. Fallahpour, "Nonuniformly spaced linear array design for the specified beamwidth/sidelobe level or specified directivity/sidelobe level with coupling consideration," *Progress In Electromagnetics Research*, Vol. 4, 185–209, 2008.